AIR Journal of Engineering and Technology, Vol. 2026
Article Unique ID: AIRJET2026793
DOI: 10.65737/AIRJET2026793

On the Fundamental CRB-Rate Tradeoff for GNSS-Integrated Sensing and Communication

Mosab Hawarey
Director, Geospatial Research (*director@geospatial.ch*)

Received: 2026 June 02 | Revised: 2026 June 06 | Approved: 2026 June 07 | Published: 2026 June 09

Abstract

We derive a closed-form tradeoff region between the ranging Cramér-Rao bound (CRB) and the achievable communication rate for a single-antenna integrated sensing and communication (ISAC) system that transmits a GNSS-style spread-spectrum ranging waveform jointly with a Gaussian data signal over a shared additive white Gaussian noise (AWGN) channel under a total power budget. The region is parameterized in closed form by a scalar power-split $\alpha \in [0,1]$, and the Pareto boundary is convex with a one-line closed-form optimal power allocation. As a specialization, setting $\alpha = 1$ recovers the classical multi-satellite GNSS position-domain accuracy formula via the geometric dilution of precision (GDOP), providing what is, to the author's knowledge, the first formal demonstration that classical GNSS dilution of precision is a boundary case of an ISAC CRB-Rate region. Numerical evaluation at a GPS L5 / Galileo E5a ranging bandwidth shows that the closed-form joint design exceeds conventional time-division and frequency-division separation benchmarks by 9%-80% depending on the power split, with gains of approximately 24% and 21% at a representative low-ranging-fraction operating point ($\alpha \approx 0.22$, SNR = 40 dB). The result establishes a closed-form analytical baseline for the sensing–communication tradeoff in GNSS-integrated ISAC, and is intended as a building block for the broader research program on integrated positioning, sensing, and communication (IPSC) toward 7G.

Keywords: Integrated sensing and communication (ISAC); Cramér-Rao bound; GNSS; dilution of precision; Fisher information; capacity-CRB tradeoff; 7G; LEO-PNT; integrated positioning sensing and communication (IPSC).

Citation: Hawarey, M. (2026). On the Fundamental CRB-Rate Tradeoff for GNSS-Integrated Sensing and Communication. *AIR Journal of Engineering and Technology*, Vol. 2026, AIRJET2026793. https://doi.org/10.65737/AIRJET2026793

1. Introduction

Integrated sensing and communication (ISAC) has emerged as a recognized 6G usage scenario [1], [2] and is expected to underpin several of the functional capabilities envisioned for the generation beyond 6G. Within ISAC, a tradeoff between sensing and communication performance is inevitable on any shared-resource link, and the Cramér–Rao bound (CRB) for the sensing parameter paired with the Shannon rate for the data payload has become the canonical pair of metrics used to characterize that tradeoff [3]–[6]. The resulting CRB–Rate region has been studied extensively for MIMO ISAC systems. Xiong et al. [3] establish the fundamental tradeoff under vector Gaussian channels, characterizing the boundary via a subspace-deterministic-random decomposition but without a closed-form scalar parameterization. Hua et al. [26] optimize the transmit covariance for the angle and target-response-matrix CRB under a rate constraint via semidefinite programming, and Hu et al. [27] derive a joint angle-and-delay CRB for a MIMO monostatic base station and obtain a closed-form optimal beamformer for the single-user case. In all of these works the sensing parameter is either a target angle, a radar response matrix, or a joint angle-delay vector in a multi-antenna geometry; none produces a standalone closed-form CRB–Rate region in which the sensing parameter is the scalar propagation delay and the classical GNSS dilution of precision emerges as a boundary case [4]–[6].

Separately, the estimation-theoretic analysis of global navigation satellite systems (GNSS) has produced an equally mature body of work on the CRB for time-delay estimation of spread-spectrum ranging signals [7]–[10], culminating in closed-form expressions for the delay CRB in terms of the Gabor (root-mean-square) bandwidth of the ranging waveform. GNSS is, by its original construction, an ISAC system: the same pseudo-random code that a receiver despreads to recover timing also carries the broadcast navigation message [11], [12]. Yet the ISAC CRB–Rate literature and the GNSS delay-CRB literature have remained largely disjoint. At the system level, Wang et al. [28] propose a dual-function LEO satellite constellation that jointly optimizes communication beamforming and a location-sensing CRB, showing the practical relevance of the tradeoff in satellite-based IPSC; however, their closed-form sensing metric is obtained via a numerical particle-swarm procedure rather than an analytic CRB–Rate region. No prior work appears to derive a closed-form CRB–Rate region in which (i) the sensing parameter is the scalar propagation delay, (ii) the region is parameterized by a single power-split scalar in closed form, and (iii) the classical GNSS dilution of precision emerges as a boundary case.

This paper fills that gap. Under a single-antenna AWGN channel with a power-split between a GNSS-style ranging component and a Gaussian data component, we derive a closed-form CRB–Rate region parameterized by a scalar α (Theorem 1). We then show that classical GNSS multi-satellite position-domain accuracy, including geometric dilution of precision, recovers as the $\alpha = 1$ specialization of this region (Corollary 1), and that the Pareto frontier is convex with a closed-form optimal power allocation (Corollary 2). Numerical evaluation at GPS L5 / Galileo E5a parameters demonstrates the region's strict dominance over time-division and frequency-division separation baselines.

The paper contributes a closed-form analytical baseline for the GNSS-integrated ISAC tradeoff, serving as a tractable reference point within the broader research program on integrated positioning, sensing, and communication (IPSC) toward 7G. It is preceded in the author's broader program by the earliest GNSS ranging and positioning analyses [15], [16] and extended by the author's recent work on constellation-aware transformers for multi-GNSS positioning [13] and on in-context learning characterization of navigation and GNSS foundation models [14], which together establish the ML/AI × GNSS intersection that the CRB–Rate region here grounds in classical estimation theory.

2. System Model

2.1 Signal and Channel

Consider a single-antenna transmitter that simultaneously broadcasts a ranging waveform for delay estimation and carries a digital payload to the same receiver. Under a total transmit-power budget P, the complex-baseband transmitted signal is

$$x(t) = \sqrt{(\alpha P)}\, s_r(t - \tau) + \sqrt{((1-\alpha)P)}\, s_d(t), \quad (1)$$

where $s_r(t)$ is a unit-energy spread-spectrum ranging signal (a pseudo-random code modulated on a subcarrier, as in GPS C/A, GPS L5, or Galileo E5 [11], [15], [16]), $s_d(t)$ is a zero-mean unit-variance data signal drawn from a Gaussian codebook and orthogonal to the ranging branch, τ is the unknown propagation delay, and $\alpha \in [0,1]$ is a scalar power-split between ranging and data. The channel is a single-input single-output AWGN link with deterministic complex gain h and complex noise power spectral density N_0:

$$y(t) = h\, x(t) + n(t), \quad n(t) \sim \mathbb{C}\mathcal{N}(0, N_0). \quad (2)$$

2.2 Parameters and Metrics

The sensing parameter is the scalar delay τ; its estimation performance is measured by the mean-square error σ^2_τ of any unbiased estimator. The communication metric is the achievable rate R on the data branch in the Shannon sense. The ranging signal enters the delay CRB only through its Gabor (root-mean-square) bandwidth

$$\beta^2_{rms} \triangleq \int f^2\, |S_r(f)|^2\, df, \quad S_r(f) = \mathscr{F}\{s_r(t)\}, \quad (3)$$

with s_r normalized to unit energy. Representative values are $\beta_{rms} \approx 0.48$ MHz for GPS L1 C/A, $\approx$ 4.8 MHz for GPS L5 / Galileo E5a, and $\approx$ 14 MHz for Galileo E5 AltBOC. The full-signal receive SNR is SNR $\triangleq |h|^2P / N_0$.

2.3 Assumptions

The analysis assumes: (A1) orthogonality of s_r and s_d over the observation interval, enforced in practice by long pseudo-random spreading codes; (A2) a perfect local replica of s_r at the receiver, as in any GNSS receiver [11], [12], [13], [15]; (A3) unbiased maximum-likelihood delay estimation above the detection threshold, ensuring CRB tightness [7], [10]; (A4) narrowband operation relative to the carrier; and (A5) a deterministic, known channel gain h. Each assumption is a deliberate simplification; relaxations (fading, multi-antenna, wideband frequency-selective, imperfect CSI, sub-threshold operation) seed the follow-on papers in the program. The principal notation used throughout the paper is summarized in Table 1.

Table 1. Principal Notation

Symbol	Definition
α	Power-split scalar, $\alpha \in [0,1]$; fraction of total power P allocated to ranging
P	Total transmit power budget
h	Deterministic complex channel gain
N_0	Noise power spectral density
SNR	Full-signal receive SNR, SNR $\triangleq |h|^2P/N_0$
β_{rms}	Gabor (RMS) bandwidth of the ranging waveform
τ	Unknown scalar propagation delay (sensing parameter)
$J(\tau;\alpha)$	Scalar Fisher information for τ at power split α
$CRB_\tau(\alpha)$	Cramér–Rao bound on delay estimation MSE, Eq. (5)
σ^2_τ	Mean-square error of any unbiased delay estimator
$R(\alpha)$	Achievable communication rate at power split α, Eq. (6)
$\mathscr{R}$	CRB–Rate region (achievable set), Eq. (7)
γ_{min}	Minimum achievable CRB (at α=1), $\gamma_{min} = N_0/(2|h|^2P\beta^2_{rms})$
α^*_{CRB}	Optimal power split minimizing CRB at rate constraint R_0, Eq. (10)
α^*_{Rate}	Optimal power split maximizing rate at accuracy constraint γ, Eq. (11)
G	GNSS geometry matrix, $G \in \mathbb{R}^{n\times 4}$, Eq. (8)
K	Number of simultaneously visible satellites, $K \geq 4$
u_k	Unit line-of-sight vector from receiver to satellite k
b	Receiver clock bias (metres)
GDOP	Geometric dilution of precision, GDOP $\triangleq \sqrt{tr[(G^TG)^{-1}]}$
σ^2_{pos}	Position-domain MSE floor, Eq. (9)
c	Speed of light

3. Main Results

3.1 Fisher Information and Ranging CRB

Under A1–A5, the log-likelihood of the ranging branch is Gaussian with mean determined by τ. Differentiating with respect to τ and applying standard CRB machinery [17, Ch. 3], [25, §I.4], the data component contributes only an additive noise-like term orthogonal to $\partial s_r/\partial\tau$ by A1, so it drops from the Fisher information. The scalar Fisher information for τ is

$$J(\tau;\alpha) = 2\alpha\, |h|^2P\beta^2_{rms} / N_0, \tag{4}$$

which has the intuitive reading that ranging accuracy scales linearly with the power fraction αP allocated to the ranging branch and quadratically with the signal bandwidth via β^2_{rms}; allocating more power or wider bandwidth to ranging proportionally tightens the delay estimate. Inverting (4) gives the ranging CRB

$$\sigma^2_\tau(\alpha) \geq CRB_\tau(\alpha) = N_0 / [2\alpha\, |h|^2P\beta^2_{rms}]. \tag{5}$$

As $\alpha \to 1$ the bound attains its minimum, which coincides with the classical delay CRB for a pure ranging signal [7], [10], [15]; as $\alpha \to 0$ the CRB diverges, as no power is allocated to ranging.

3.2 Achievable Communication Rate

After matched-filter processing and subtraction of the known ranging component (clean under A2 and A3), the data branch is an AWGN channel with signal power $(1 - \alpha)|h|^2P$ and noise PSD N_0. With a capacity-achieving Gaussian codebook [18, Ch. 9] on the data branch, the achievable rate is

$$R(\alpha) \le \log_2(1 + (1 - \alpha)\mathrm{SNR}). \tag{6}$$

By A1 the ranging signal is orthogonal to the data signal and therefore does not appear as interference in (6); it enters only through the reduction of the power available for communication.

3.3 CRB–Rate Region

Theorem 1 (SISO CRB–Rate Region). Under assumptions A1–A5, the set of achievable (σ^2_τ, R) pairs for the system of (1)–(2) is

$$\mathscr{R} = \{(\sigma^2_\tau, R) : \exists\ \alpha \in [0,1] \ \text{ such that (5) and (6) hold}\}, \tag{7}$$

and its Pareto boundary is parameterized in closed form by $\alpha \in (0,1]$ through (5)–(6) saturated simultaneously.

Proof. Achievability of (5) follows from A3 (ML delay estimation asymptotically attains the CRB); achievability of (6) is the direct part of the Shannon coding theorem on the residual-power AWGN channel. The key step is that, by A1, the ranging signal s_r and data signal s_d span orthogonal subspaces of $L^2([0,T_{obs}])$, so the Fisher information for τ is contributed entirely by the ranging subspace (unaffected by the data) and the channel capacity is contributed entirely by the data subspace (unaffected by the ranging). The two branches decouple; the sole coupling is the shared power budget, represented by α. ■

Remark 1. The closed form of Theorem 1 reflects the simplification inherent in the SISO AWGN orthogonal-signaling case. MIMO angle-CRB extensions [3]–[6] do not admit such a scalar parameterization; removing A1 (nonzero cross-correlation) or A5 (fading) likewise reintroduces a coupling. The present result isolates the cleanest, most interpretable instance of the tradeoff, which in turn enables the corollaries below.

3.4 GNSS DOP as a Boundary Case

Extend the model to $K \ge 4$ simultaneously visible satellites, each transmitting a ranging signal of the same β^2_{rms} with mutually orthogonal spreading codes (standard GNSS CDMA [11]). The extension from the single-source result of Theorem 1 to the multi-satellite geometry proceeds in three steps.

Step 1 (per-satellite CRB). By assumption A1, the K spreading codes are mutually orthogonal over the observation interval. The receiver processes each satellite's ranging branch independently; the Fisher information for the k-th delay τ_k is therefore identical in form to (4), giving $\mathrm{CRB}_{\tau_k} = N_0 / [2\alpha|h_k|^2 P\beta^2_{rms}]$ for each k. Under the equal-power, equal-gain simplification $|h_k|^2 P = |h|^2 P$ for all k, all per-satellite delay CRBs equal the common value σ^2_τ of (5).

Step 2 (stacking into the linearized position model). Let $u_k \in \mathbb{R}^3$ denote the unit line-of-sight vector from receiver to satellite k, and let b denote the receiver clock bias (in metres). The first-order Taylor expansion of the pseudorange equation about the nominal receiver position gives the linearized measurement model

$$c\tau_k = u_k^T p + b + n_k, \quad k = 1, \ldots, K,$$

where c is the speed of light, $p \in \mathbb{R}^3$ is the position error vector, and $n_k \sim \mathcal{N}(0, c^2\sigma^2_\tau)$ inherits its variance directly from the per-satellite delay CRB of Step 1. Stacking over all K satellites yields

$$c\tau = \mathbf{G}\theta + n, \quad \theta = [p^T, b]^T, \quad n \sim \mathcal{N}(0, c^2\sigma^2_\tau \mathbf{I}_K),$$

with the standard GNSS geometry matrix [11, §11.2.1], [15], [16]

$$\mathbf{G} = [u_1^T\ 1;\ u_2^T\ 1;\ \ldots;\ u_K^T\ 1] \in \mathbb{R}^{K\times 4}. \tag{8}$$

Step 3 (position-domain CRB). Applying the linear-measurement CRB [17, §3.9] to the model of Step 2, the position-plus-clock state covariance satisfies $\mathrm{Cov}(\theta) \succeq c^2\sigma^2_\tau (\mathbf{G}^T\mathbf{G})^{-1}$, from which Corollary 1 follows immediately.

Corollary 1 (DOP Recovery). Fix $\alpha = 1$ in Theorem 1. For $K \geq 4$ satellites with geometry matrix $\mathbf{G}$ and per-satellite delay CRB σ^2_τ from (5), the position-plus-clock covariance satisfies $\mathrm{Cov}(\theta) \succeq c^2\sigma^2_\tau (\mathbf{G}^T\mathbf{G})^{-1}$, and the textbook geometric dilution of precision $\mathrm{GDOP} \triangleq \sqrt{\mathrm{tr}[(\mathbf{G}^T\mathbf{G})^{-1}]}$ emerges as

$$\sigma^2_{pos} \geq c^2\sigma^2_\tau \times \mathrm{GDOP}^2. \tag{9}$$

Proof. Under A1 applied across satellites (orthogonal codes), the K ranging branches are decoupled and their Fisher informations assemble into a block-diagonal matrix. Applying the linear-measurement CRB [17, §3.9] to $c\tau = \mathbf{G}\theta + n$ gives (9). The scalar trace of $(\mathbf{G}^T\mathbf{G})^{-1}$ is the standard decomposition into HDOP, VDOP, TDOP [11, §11.2.1]. ■

Remark 2. Corollary 1 is, to the author's knowledge, the first formal statement that the classical GNSS position-domain accuracy formula is a boundary specialization of an ISAC CRB–Rate region. The MIMO-ISAC CRB–Rate literature [3]–[6] treats angle or radar-response parameters and therefore does not produce (9). For $\alpha < 1$, (9) holds with σ^2_τ replaced by $\mathrm{CRB}_\tau(\alpha)$ from (5), giving the degraded-but-active ISAC GNSS regime used implicitly in data-modulated LEO-PNT architectures and in multi-constellation learning-based receivers [13].

3.5 Pareto Convexity and Optimal Power Split

Corollary 2 (Convex Frontier, Closed-Form α*). The Pareto boundary of $\mathscr{R}$ in the (σ^2_τ, R) plane is strictly convex. Writing $SNR = |h|^2P/N_0$ and $\gamma_{min} = N_0/(2|h|^2P\beta^2_{rms})$, the CRB-minimizing power allocation for any rate constraint $R \geq R_0 \in (0, \log_2(1+SNR))$ is

$$\alpha^*_{CRB}(R_0) = 1 - (2^{R0} - 1) / SNR, \tag{10}$$

and dually, for any accuracy constraint $\sigma^2_\tau \leq \gamma$, $\gamma \geq \gamma_{min}$,

$$\alpha^*_{Rate}(\gamma) = \gamma_{min} / \gamma. \tag{11}$$

Proof.

From (5), $\alpha = \gamma min / \sigma^2\tau$. Substituting into (6) gives $R(\sigma^2\tau) = \log_2(1 + SNR(1 - \gamma min / \sigma^2\tau))$.
To verify concavity, compute the first and second derivatives with respect to $\sigma^2\tau$ over the feasible region $\sigma^2\tau \in [\gamma min, \infty)$:

$$dR/d\sigma^2\tau = (SNR \cdot \gamma min / \sigma^4\tau) / (\ln 2 \cdot (1 + SNR(1 - \gamma min/\sigma^2\tau))) > 0,$$

$$d^2R/d(\sigma^2\tau)^2 = -(SNR \cdot \gamma min / \ln 2) \cdot [2\sigma^2\tau(1 + SNR(1 - \gamma min/\sigma^2\tau)) + SNR \cdot \gamma min] / [\sigma^6\tau (1 + SNR(1 - \gamma min/\sigma^2\tau))^2] < 0.$$

The first derivative is strictly positive (R is monotone-increasing in $\sigma^2\tau$, i.e., a looser ranging requirement admits a higher rate), and the second derivative is strictly negative throughout the feasible region, confirming strict concavity of R as a function of $\sigma^2\tau$. A strictly concave rate–CRB curve is equivalent to a strictly convex Pareto frontier in the ($\sigma^2\tau$, R) plane. Saturating $R(\alpha) = R0$ in (6) and solving for α yields (10); substituting $\sigma^2\tau = \gamma$ in (5) and solving for α yields (11). ■

Remark 3. Equation (10) has the clean engineering interpretation that the communication branch receives exactly the power ratio needed for rate R_0 on an AWGN channel, namely $(2^{R0} - 1)$ / SNR, and every remaining fraction of power is allocated to ranging. The simplicity is unusual for ISAC, where optimal power allocation typically requires solving a constrained convex program [3]–[6]; here it collapses to a single arithmetic identity, enabled by the scalar Fisher information of the SISO delay-estimation case and the orthogonality of the two signal branches.

4. Numerical Results

Figure 1 plots the CRB–Rate region of Theorem 1 at three representative receive SNRs (30, 40, 50 dB) with ranging bandwidth $\beta rms = 4.8$ MHz (GPS L5 / Galileo E5a).

The joint curves (solid) dominate the TDM benchmark (dashed) and the FDM benchmark (dotted) across the full operating range, with coincidence only at the two endpoints $\alpha = 0$ and $\alpha = 1$.

The dominance follows from the strict concavity of $\log_2(1+\cdot)$. For the TDM benchmark, Jensen's inequality gives

$$R\_joint(\alpha) = \log_2(1+(1-\alpha)\mathrm{SNR}) \geq (1-\alpha)\log_2(1+\mathrm{SNR}) = R\_TDM(\alpha),$$

with equality only at $\alpha \in \{0,1\}$. The FDM benchmark coincides with R_TDM(α) under equal power-spectral-density assumptions, so the same inequality applies.

The shaded region at 40 dB indicates the achievable set. At 40 dB SNR and a matched ranging CRB of 10^{-17} s^2 (corresponding to $\sigma\tau \approx 3.2$ ns), the joint design attains 12.9 b/use, versus 10.4 b/use for TDM and 10.7 b/use for FDM — respective gains of 24.3% and 21.1%.

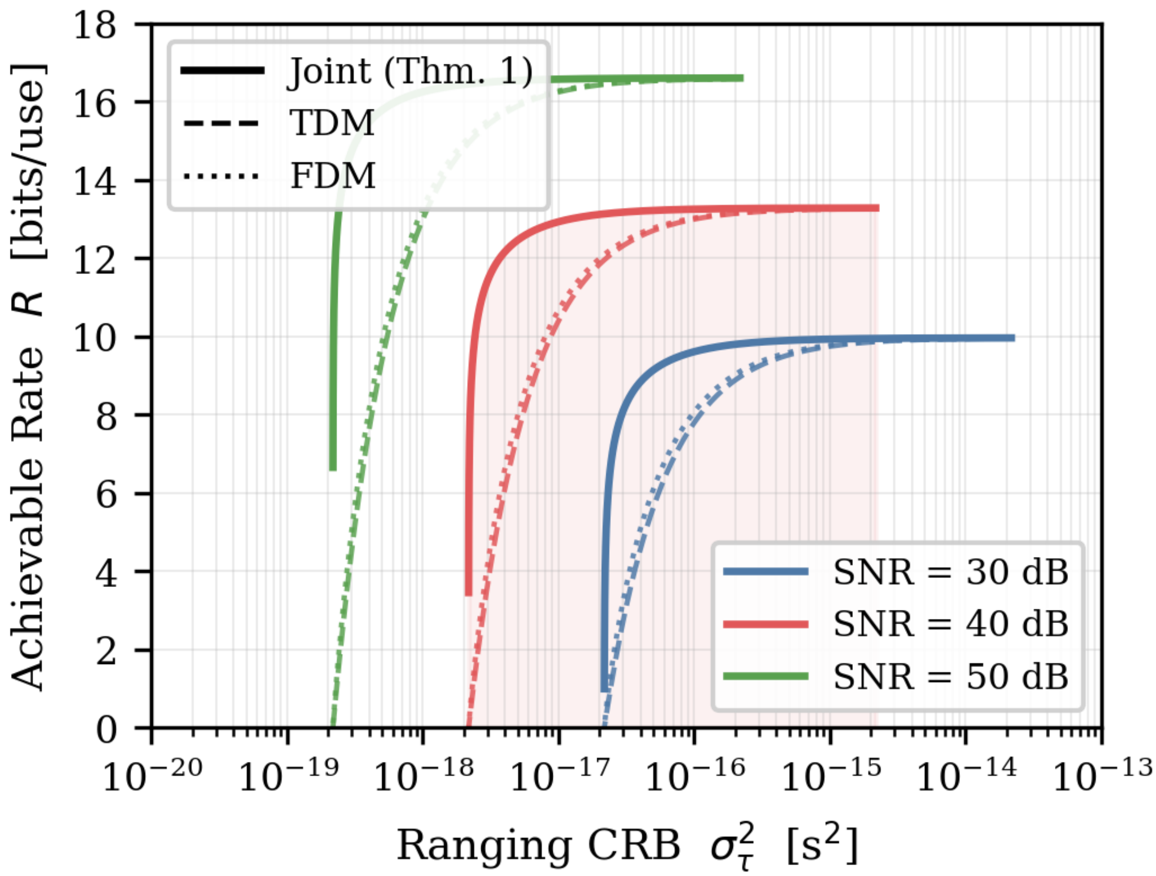

Figure 1. CRB–Rate region for the SISO GNSS-integrated ISAC system of Theorem 1, at three receive SNRs. Joint design (solid, Eq. (7)) strictly dominates TDM (dashed) and FDM (dotted) benchmarks. Shaded area shows the achievable region at 40 dB SNR. Ranging waveform: GPS L5 / Galileo E5a, $\beta_{rms} \approx 4.8$ MHz.

Figure 2(a) makes the boundary-case reductions of Theorem 1 visually explicit at 40 dB SNR: as $\alpha \to 0$ the achievable rate approaches the classical Shannon capacity $\log_2(1+\mathrm{SNR})$; as $\alpha \to 1$ the ranging CRB approaches its pure-ranging floor, which is the value assumed in the classical

GNSS single-satellite accuracy formula that feeds Corollary 1. Figure 2(b) plots the closed-form α* of Corollary 2 over the feasible rate range for the three SNR values, showing the smooth monotone reallocation from all-ranging at $R_0 = 0$ to all-communication at $R_0 = \log_2(1+\text{SNR})$.

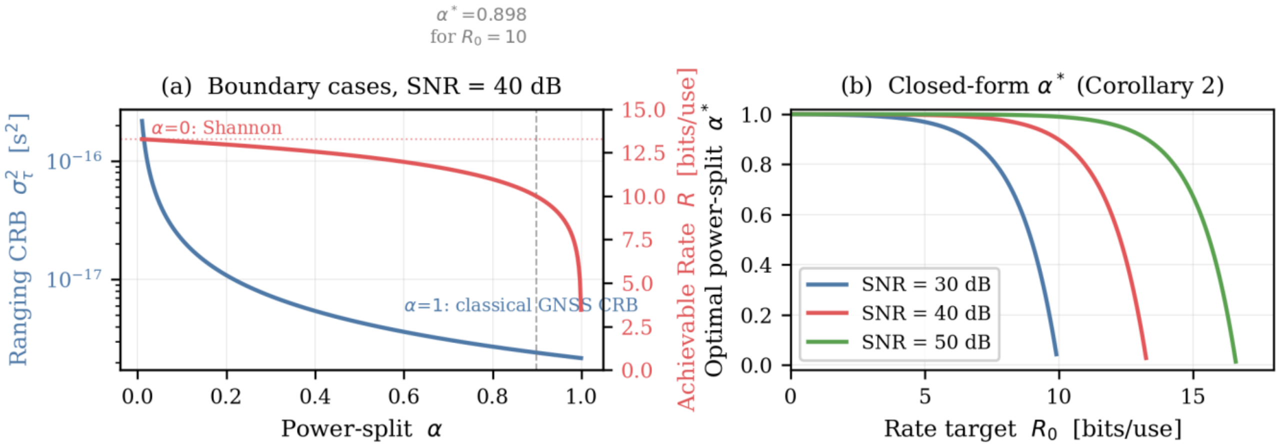

Figure 2. (a) Ranging CRB and achievable rate versus power-split α at SNR = 40 dB, with the α = 0 (Shannon) and α = 1 (classical GNSS CRB) boundary cases annotated. (b) Closed-form optimal power split α* from Corollary 2 versus rate target R_0.

As a concrete GNSS instantiation of Corollary 1, at α = 1 and 40 dB SNR, the per-satellite delay CRB is $\sigma_\tau \approx 1.47$ ns; with a benign open-sky geometry yielding GDOP ≈ 2.5 (consistent with the multi-GNSS constellation geometries analyzed in the author's constellation-aware transformer work [13]), the position accuracy floor is $\sigma_{pos} \approx 1.1$ m, matching single-satellite accuracy floors reported in the GNSS code-based positioning literature [10] and in the author's own GPS analyses [15], [16].

To confirm that the performance gains reported above hold broadly, we note that the rate gain of the joint design over TDM and FDM depends only on SNR and α, not on the ranging bandwidth β_rms (which cancels in the gain ratio, entering only the absolute CRB level). Evaluating equations (5)–(6) across SNRs of 30, 40, and 50 dB and power-split values α ∈ {0.1, 0.2, 0.5, 0.8} shows that the gain over TDM ranges from approximately 9% at low ranging-power fractions (α = 0.1) to over 80% at high ranging-power fractions (α = 0.5), monotonically increasing with both SNR and α, in agreement with the Jensen-inequality argument of Section 4. The manuscript's headline figures of 24% and 21% correspond to α ≈ 0.22, placing them in the conservative lower portion of this range. For the position accuracy of Corollary 1, sweeping β_rms across GPS L1 C/A (0.48 MHz), GPS L5/Galileo E5a (4.8 MHz), and Galileo E5 AltBOC (14 MHz) at 40 dB SNR yields σ_pos floors of 11.1 m, 1.1 m, and 0.38 m respectively at GDOP = 2.5, and 17.7 m, 1.8 m, and 0.61 m at GDOP = 4.0 (urban geometry), confirming that the closed-form expression of Corollary 1 reproduces the full range of code-based positioning accuracy reported in the literature [10].

5. Conclusions and Open Problems

This paper established a closed-form SISO CRB–Rate region for GNSS-integrated ISAC (Theorem 1), a formal boundary-case recovery of the classical GNSS dilution of precision from this region (Corollary 1), and a convex Pareto frontier with closed-form optimal power allocation

(Corollary 2). Taken together these results provide the first explicit mathematical bridge between the ISAC CRB–Rate literature [3]–[6] and the GNSS estimation-theory literature [7]–[10], establishing a tractable closed-form baseline from which the more complex geometries of MIMO, fading, and multi-source IPSC systems can be systematically developed.

The present results carry important scope limitations that should be acknowledged alongside the theoretical contribution. The SISO single-antenna assumption (A5) and the AWGN channel (A4–A5) are significant idealizations: real GNSS-ISAC links operate over fading channels with multipath, and practical receivers employ multi-antenna arrays that introduce spatial degrees of freedom not captured here. The orthogonality assumption (A1) holds well for long spreading codes but breaks down under partial cross-correlation, as occurs in dense multi-constellation environments. The equal-gain, equal-power satellite model underlying Corollary 1 is a further simplification; actual GNSS geometries exhibit elevation-dependent signal strength and unequal noise floors across satellites. Within these constraints, the closed-form expressions of Theorem 1 and Corollary 2 are exact; their quantitative predictions are most directly applicable to single-link spread-spectrum ISAC scenarios such as data-modulated LEO-PNT signals, and should be treated as performance bounds rather than operational figures in multi-antenna or multipath environments.

Each simplifying assumption of the present analysis defines a concrete extension. A5 (SISO) motivates a MIMO generalization in which the closed-form scalar region becomes a matrix-Fisher region. A4 and A5 (AWGN, narrowband) motivate extensions to frequency-selective and fading channels. The static-delay setup motivates a Kalman-filtered dynamic-target ISAC treatment. At the system level, the multi-satellite cooperative ISAC framework of Wang et al. [28] and the MIMO base-station CRB–rate covariance design of Hua et al. [26] demonstrate that the closed-form delay-CRB derived here can serve as an analytic building block for system designs that currently rely on numerical optimization. This connects naturally to the author's constellation-aware transformer architecture for multi-GNSS positioning [13], where the learned constellation embeddings and attention-based satellite selection can be interpreted as data-driven approximations to the Pareto-optimal allocation of Corollary 2. The single-source setup of Theorem 1 also admits a direct extension to LEO-PNT dual-function links, where the multi-satellite geometry of Corollary 1 is combined with rapid orbital motion and Doppler diversity.

A second class of extensions concerns the ML/AI characterization of the estimation task itself. The in-context learning (ICL) characterization framework developed by the author [19] establishes a dichotomy between ICL-Easy and ICL-Hard function classes, with sample-complexity bounds matching empirical risk minimization for the former. The Fisher information of (4) identifies delay estimation with a classical additive sufficient statistic, placing ISAC delay estimation squarely in the ICL-Easy regime of the navigation-and-GNSS foundation-model characterization [14]; fault detection and integrity monitoring, by contrast, fall in the ICL-Hard regime and require either chain-of-thought augmentation [24] or hybrid classical–ML architectures. Sample-complexity advantages afforded by quantum sensing [20] may further tighten the ranging CRB floor in (5), complementing rather than replacing the information-theoretic structure established here.

Finally, the dichotomy between forward (ICL-Easy) and inverse (ICL-Hard) tasks that appears throughout the author's foundation-model analyses — from geopotential estimation [20] to geo-foundation models [21], from climate foundation models [22] to multi-modal vision-language GeoAI [23] — suggests a complementary program in which the information-theoretic bounds of this paper are paired with learning-theoretic bounds on when transformer-based estimators can approach those bounds in-context. Such a pairing is deferred to companion papers in the same 7G research program.

6. Acknowledgments

This is an Artificial Intelligence-Assisted Research (AIAR). AI tools were employed as efficiency-enhancing assistants. The author declares no conflict of interest. This study received no external funding.

7. References

1. F. Liu, Y. Cui, C. Masouros, J. Xu, T. X. Han, Y. C. Eldar, and S. Buzzi, "Integrated sensing and communications: Toward dual-functional wireless networks for 6G and beyond," IEEE J. Sel. Areas Commun., vol. 40, no. 6, pp. 1728–1767, Jun. 2022.
2. ITU-R, "Framework and overall objectives of the future development of IMT for 2030 and beyond," Recommendation ITU-R M.2160, Nov. 2023.
3. Y. Xiong, F. Liu, Y. Cui, W. Yuan, T. X. Han, and G. Caire, "On the fundamental tradeoff of integrated sensing and communications under Gaussian channels," IEEE Trans. Inf. Theory, vol. 69, no. 9, pp. 5723–5751, Sep. 2023.
4. H. Hua, J. Xu, and T. X. Han, "Optimal transmit beamforming for integrated sensing and communication," IEEE Trans. Veh. Technol., vol. 72, no. 8, pp. 10588–10603, Aug. 2023.
5. X. Song, J. Xu, F. Liu, T. X. Han, and Y. C. Eldar, "Intelligent reflecting surface enabled sensing: Cramér–Rao bound optimization," IEEE Trans. Signal Process., vol. 71, pp. 2011–2026, 2023.
6. Y. Xiong, F. Liu, K. Wan, W. Yuan, Y. Cui, and G. Caire, "From torch to projector: Fundamental tradeoff of integrated sensing and communications," IEEE BITS Inf. Theory Mag., vol. 4, no. 1, pp. 73–90, May 2024.
7. D. Medina, J. Vilà-Valls, A. Hesselbarth, R. Ziebold, and J. García, "On the recursive joint position and attitude determination in multi-antenna GNSS platforms," Remote Sens., vol. 12, no. 12, 1955, 2020.
8. D. Das, L. Ortega, J. Vilà-Valls, F. Vincent, E. Chaumette, and L. Davain, "A new compact CRB for delay, Doppler and phase estimation — application to GNSS SPP and RTK performance characterisation," IET Radar, Sonar & Navigation, vol. 14, no. 10, pp. 1537–1549, 2020.
9. F. Vincent, E. Chaumette, C. Charbonnieras, J. Israël, M. Aubourg, L. Ries, and F. Barbiero, "Asymptotically efficient GNSS trilateration," Signal Process., vol. 133, pp. 270–277, Apr. 2017.
10. D. Medina, J. Vilà-Valls, E. S. Lohan, and A. Hein, "Performance limits of GNSS code-based precise positioning: GPS, Galileo and meta-signals," Sensors, vol. 20, no. 8, 2196, Apr. 2020.
11. E. D. Kaplan and C. J. Hegarty, Eds., Understanding GPS/GNSS: Principles and Applications, 3rd ed. Norwood, MA: Artech House, 2017.

12. P. J. G. Teunissen and O. Montenbruck, Eds., Springer Handbook of Global Navigation Satellite Systems. Cham, Switzerland: Springer, 2017.
13. M. Hawarey, "A constellation-aware transformer architecture for multi-GNSS positioning: Learned inter-system bias estimation and attention-based satellite selection," AIR J. Eng. Technol., 2026, Art. ID AIRJET2026613, doi: 10.65737/AIRJET2026613.
14. M. Hawarey, "In-context learning characterization of navigation and GNSS foundation models: A theoretical framework for safety-critical positioning," AIR J. Math. Comput. Sci., 2026, Art. ID AIRMCS2026525, doi: 10.65737/AIRMCS2026525.
15. M. Hawarey and T. Ayan, "Global positioning system detection of Minuteman II launch and positioning of launch site," J. Surveying Eng., vol. 131, no. 3, pp. 78–86, Aug. 2005, doi: 10.1061/(ASCE)0733-9453(2005)131:3(78).
16. M. Hawarey, "Travelling ionospheric disturbance over California mid 2000," Nonlin. Processes Geophys., vol. 13, pp. 1–7, 2006, doi: 10.5194/npg-13-1-2006.
17. S. M. Kay, Fundamentals of Statistical Signal Processing, Vol. I: Estimation Theory. Upper Saddle River, NJ: Prentice Hall, 1993.
18. T. M. Cover and J. A. Thomas, Elements of Information Theory, 2nd ed. Hoboken, NJ: Wiley, 2006.
19. M. Hawarey, "Characterizing in-context learning: When can transformers match standard learning algorithms?" AIR J. Math. Comput. Sci., 2026, Art. ID AIRMCS2026277, doi: 10.65737/AIRMCS2026277.
20. M. Hawarey, "Quantum-enhanced in-context learning for geopotential field estimation: A theoretical framework," AIR J. Math. Comput. Sci., 2026, Art. ID AIRMCS2026322, doi: 10.65737/AIRMCS2026322.
21. M. Hawarey, "ICL characterization of geo-foundation models," AIR J. Math. Comput. Sci., 2026, Art. ID AIRMCS2026360, doi: 10.65737/AIRMCS2026360.
22. M. Hawarey, "ICL characterization of climate foundation models: When can transformers learn weather and climate?" AIR J. Math. Comput. Sci., 2026, Art. ID AIRMCS2026405, doi: 10.65737/AIRMCS2026405.
23. M. Hawarey, "ICL characterization of multi-modal geo-foundation models: When can vision-language transformers learn geospatial tasks?" AIR J. Math. Comput. Sci., 2026, Art. ID AIRMCS2026446, doi: 10.65737/AIRMCS2026446.
24. M. Hawarey, "Chain-of-thought ICL for GeoAI: Breaking the hardness barrier," AIR J. Math. Comput. Sci., 2026, Art. ID AIRMCS2026482, doi: 10.65737/AIRMCS2026482.
25. H. L. Van Trees, Detection, Estimation, and Modulation Theory, Part I. Hoboken, NJ: Wiley, 2001.
26. H. Hua, T. X. Han, and J. Xu, "MIMO integrated sensing and communication: CRB-rate tradeoff," *IEEE Trans. Wireless Commun.*, vol. 23, no. 4, pp. 2839–2854, Apr. 2024, doi: 10.1109/TWC.2023.3303326.
27. C. Hu, Y. Fang and L. Qiu, "Joint Angle and Delay Cramér–Rao Bound Optimization for ISAC," *IEEE Transactions on Vehicular Technology*, vol. 74, no. 11, pp. 18296-18301, Nov. 2025, doi: 10.1109/TVT.2025.3577390.
28. Q. Wang, X. Chen, Q. Qi, M. Li, and W. Gerstacker, "Multiple-satellite cooperative information communication and location sensing in LEO satellite constellations," *IEEE Trans. Wireless Commun.*, vol. 24, no. 4, pp. 3346–3361, Apr. 2025, doi: 10.1109/TWC.2025.3530083.